Scientia Iranica A (2022) 29(6), 2886–2901

Sharif University of Technology
Scientia Iranica
Transactions A: Civil Engineering
http://scientiairanica.sharif.edu

Effect of hydrochloric acid corrosion and CFRP coating on the buckling behavior of cylindrical shells under external pressure

A.C. Aydin[a,*], M.B. Bilen[b], and M. Maali[b]

a. *Department of Civil Engineering, Engineering Faculty, Ataturk University, Erzurum, Turkey.*
b. *Department of Civil Engineering, Architecture and Engineering Faculty, Erzurum Technical University, Erzurum, Turkey.*

Received 25 January 2021; received in revised form 9 May 2021; accepted 6 December 2021

KEYWORDS
Cylindrical shell;
HCI;
CFRP;
Experimental;
Uniform external pressure.

Abstract. Thin-walled cylindrical shells are widely used as silos, liquid tanks, marine structures, and industrial chemical plants. In such applications, the shells are mostly exposed to liquids. Corrosion occurs on surfaces when shells are filled with low-pH liquids. Corroded material loss decreases the thickness of the shells which in turn lessens their buckling capacity. The current study primarily aims to investigate the effects of corrosion on the buckling capacity of thin-walled cylindrical shells subjected to uniform external pressure. The model shells were half- or full-filled with 5% and 10% HCl (Hydrochloric Acid) solutions for corrosion. In order to attenuate the negative effects of corrosion, the cylinders were coated with varying sizes of Carbon Fiber-Reinforced Polymer (CFRP) sheets. A total of 12 models of $800 \times 400 \times 0.45$ mm in dimension were investigated in this research. The perfect non-corroded models were employed to compare the behavior of all models under study. The obtained results indicated that corrosion would cause a significant decrease in the buckling capacity of thin-walled cylindrical shells. It should be noted that the acid ratio, filling rate, and surface area coated with CFRP fabrics considerably affected the buckling capacity of cylinders. To be specific, coating the cylinders with one layer of CFRP moderated the buckling capacity loss.

1. Introduction

Corrosion is the process of returning the unstable metals to their original state in an atmospheric environment. When a metal interacts with hydrochloric acid, hydrogen ions take the electrons the metal loses through oxidation. In this electron exchange on the metal surface, the areas where the electrons are being given up are called anodes and the areas where the electrons are being absorbed are called cathodes. While the negatively charged ions move from the anode to cathode, the positively charged hydrogen ions move from cathode to anode, thus causing corrosion on the metal surface [1]. The most common effect of corrosion on the steel is the material loss on its surface which in turn decreases its strength [2–4]. Numerous researches have thoroughly investigated this issue in the literature. For instance, Sharifi and Rahgozar [5] examined the corrosion damages in three steel I-beams used in the petrochemical industry. They stated that the shear capacity of steel profiles decreased due to corrosion. Lugauskas et al. [6] studied the corrosion behavior of low-carbon steel and aluminum in the external

*. *Corresponding author. Tel.: +90 5306786101*
Fax: +90 4422314910
E-mail addresses: acaydin@atauni.edu.tr (A.C. Aydin); mahmut.bilen@erzurum.edu.tr (M.B. Bilen); mahyar.maali@erzurum.edu.tr (M. Maali)

doi: 10.24200/sci.2021.57618.5332

environment in rural, marine, and industrial areas. Corrosion of steel and aluminum materials depends on the atmospheric corrosion level of the environment. In this respect, Çelik [7] examined the corrosion behavior of austenitic stainless steels in his study. The levels of local corrosion resistance of austenitic stainless steels such as pitting and crevice corrosion were found to be low. Of note, corrosion of this material in the body can cause several health problems. Qiao [8] examined pipelines with small diameter and observed that the corrosion reduced the thickness of pipelines over time, leading to cracks and failures. Manliza [9] examined the corrosion and cavitation of water pipes in Hong Kong. According to their findings, corrosion seriously damages the pipe material and poses a health risk if it interacts with drinking water. Becerra et al. [10] evaluated the effect of oil content on the corrosion of AISI-SAE 1010 carbon steel in oil-in-water emulsions. Electrochemical activity decreases with an increase in the oil content. They stated that in low emulsions with a low content of oil ($< 20 - 40\%$), as the oil content increases, the corrosion rate increases. Patané et al. [11] studied an air cylinder damaged by corrosion. The CO_2 content in the condensed water in the pressurized gas storage tanks decreases the pH value of the water and water with increased acidity causes corrosion in the tank. Kong et al. [12] evaluated the galvanic corrosion behavior of an underwater joint in their study. Given the difference between the weld and base metals, the junction areas are vulnerable to galvanic corrosion. Chegeni et al. [13] studied the effects of corrosion depth and shape on the performance of thin-walled steel tubes through numerical and experimental methods. The tubes were subjected to combined internal pressure and four-point bending load. They stated that the bending capacity decreased as the corrosion depth increased. In addition, as the surface area affected by corrosion increased, the bending capacity decreased. Zhao et al. [14] investigated the effects of pitting corrosion on the bending capacity of thin-walled cylindrical tubes based on nonlinear numerical analysis. They simulated corrosion by reducing the cylinder thickness. The corrosion shape affected the bending capacity and buckling caused by corrosion, which decreased the bending capacity.

Shells are often used in the submarines, missiles, tanks, and liquid reservoirs [15,16]. Therefore, it is important to examine the buckling behavior under different effects [17]. Maali et al. [18] and Kılıç and Çinar [19] investigated the effect of size and imperfections on the buckling capacity of shells in their study. They observed that the effect of imperfection would become even more tangible as the height increased. Fatemi et al. [20] examined the buckling behavior of four groups of specimens with different measures and imperfection magnitudes in their study. In addition, upon increasing the depth of the initial imperfection, the buckling capacity decreased. Being quite sensitive, such structures are significantly affected by initial imperfections. Niloufari et al. [21] examined the effect of weld-induced geometric imperfections on the buckling capacity of shells. They studied 12 specimens with different ratios of t/R (where R is the radius of the tanks and t the thickness) tested under hydrostatic pressure. Geometrical imperfections at different t/R ratios may have either decreasing or increasing effects on the buckling capacity of the cylinders.

Fiber-Reinforced Polymer (FRP) composites are widely used to strengthen the materials with their high strength-to-weight ratio and high corrosion resistance [22–25]. FRP composites with fibers oriented in the circumferential direction can be used to prevent possible buckling of shells. For circular steel tubes, external FRP confinement is an effective method [26]. In addition, Carbon Fiber-Reinforced Polymer (CFRP) as an effective method can be employed to strengthen the damaged steel structures [27]. Li et al. [28] examined the bond between the CFRP plates and corroded steel plates. They found that the effect of the adhesive thickness on deformation was higher than that of the corrosion time by examining samples at different corrosion times and adhesive thicknesses. For corrosion, sodium chloride solution was sprayed for five minutes every four hours. Maali et al. [29] investigated the effect of dent and CFRP on the buckling behavior of thin-walled steel cylindrical shells. They studied 14 specimens in two groups: with and without CFRP. Dents were placed in different directions and the buckling behavior was examined under an external pressure. They observed that the buckling capacity of the cylinders increased with CFRP reinforcement. Teng and Hu [30] examined the reinforcement of steel pipes using the FRP. Steel pipes were coated with FRP in three layers and tested under an axial pressure. As the thickness of the FRP reinforcement increased, the ductility of the steel pipes increased significantly. However, since this increase in thickness loses its effect when the pipes start to buckle from the inside, there is a limited increase in buckling capacities. Ghazijahani et al. [31] investigated the effect of the CFRP on the buckling capacity of timber filled thin-walled steel cylinders. The CFRP reinforced the cylinder, thus protecting it against external buckling. Inward buckling behavior took control because CFRP failed to be effective as it was in external buckling. The CFRP roller strengthened the cylinders against the buckling style known as elephant foot buckling.

The current research evaluates the buckling behavior of 12 thin-walled cylindrical shells in direct exposure to uniform external pressure. In this regard, ten models were corroded in 5% and 10% HCl solutions, and the other two models without corrosion were tested. In addition, CFRP with different lengths of

800 mm, 400 mm, and 100 mm were coated on the cylinders to withstand the effects of corrosion. The cylinders were weighed before and after corrosion to calculate the total weight loss. All tests in this research were carried out at the Steel Structural Lab of Atatürk University, Erzurum, Turkey. The buckling loads were compared and estimated according to the theoretical loads of Jawad [32], Venstel and Krauthammer [33], and Ross [34]. However, the mentioned theories were not designed to determine the corroded steel tanks, as in this work.

2. Test setup and models

2.1. Preparation of the test setup and cylinders

In this research, an experimental setup was prepared for use, as shown in Figure 1. The test setup consists of two steel plates with the dimensions of 1500 × 1500 mm and thickness of 30 mm. These plates were then cut into the exact dimensions using CNC cutting machine. Circular supports were then welded to the plates where the rollers would be placed. Two holes were formed in the middle of the top plate, one for the vacuum pipe and another in the load cell. In order to control the movement of the upper plate, total of six holes were opened, four on the corners of the plates, and two in the middle of the edges. Bolts were placed in these holes. After the preparation of the test setup, the preparation of the test models was initiated. Three tensile coupon tests were performed to obtain the properties of the material. Based on the test results, the failure and yield stresses were found 342.4 MPa and 198.8 MPa. Modulus of elasticity and Poisson ratio were 210 GPa and 0.29, respectively. To prepare 12 cylinder models with the dimensions of $800 \times 400 \times 0.45$ mm, rectangular steel sheets with the dimensions of 1260×800 mm and thickness of 0.45 mm were used. The sheets were rolled

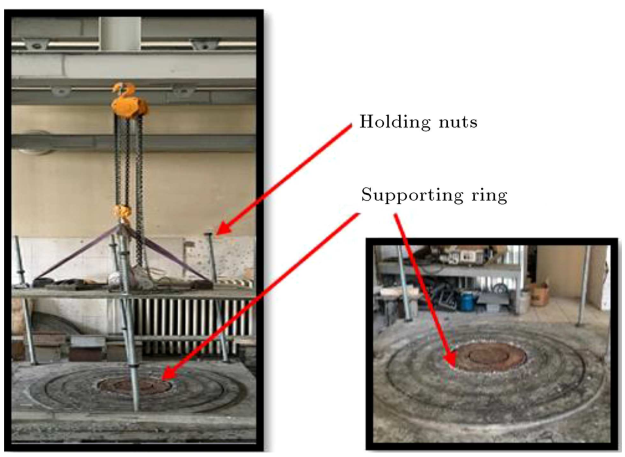

Figure 1. Vacuuming experimental setup for thin-walled steel cylinders.

Figure 2. Filling cylinders with HCl solution.

by the machine used by Maali et al. [35] and Aydın et al. [36]. The joints of the cylinders were attached to each other by soldering. The reason behind using the soldering method for the joints is as it provides an advantage in the construction and experiment phases. Soldering is both economic and prevents the possible damage to thin material [17].

2.2. Corrosion tests

After the preparation of the cylinders, the preparation phase in the corrosion test was initiated. First, the rollers were weighed before corrosion and noted. To keep the aqueous acid solution in the cylinders without any leaks, cylinders were put on the foam boards. The foam boards were used given their impermeability and were affected by hydrochloric acid. The cylinders were put on the foam boards firmly and the contact area of the cylinder and foam board were glued with silicon from inside and outside to ensure there are not any leaks. After waiting for the 24-hour period for silicon glue to get dry, cylinder's impermeability was checked by filling the cylinder with some water. Then, water and acid were filled with the determined ratios, as shown in Figure 2. In this study, hydrochloric acid with a purity of 30–32% and a density of 1.15–1.16 g/cm^3 was used to corrode the cylinders. The ratio of hydrochloric acid used is presented in Table 1. The reason for using the acid as 5% and 10% solutions is that it is the general acidic effect taken under consideration for varying purposes in the literature [1,4,7,9,10]. After filling the cylinders with solutions, the cylinders were kept at room temperature for a day to complete the corrosion. At the end of the period, the solution was safely emptied and the cylinders were cleaned. After cleaning, cylinders were weighed again and the weight loss caused by corrosion was determined.

2.3. Applying CFRP to the cylinders

After the completion of the corrosion, MasterBrace P 3500 branded special epoxy primer was applied to the outer surface of the cylinders with the help of roller to make CFRP coating. The two parts of the epoxy primer

Table 1. Model properties.

Model	Fulness	HCl solution (%)	CFRP height (mm)	Weight of the model (g)	
				Non-corroded	Corroded
Perfect model	–	–	–	–	–
Perfect model with whole surface CFRP	–	–	800 (Full height)	–	–
M1–F–A10–CN	Full	10%	–	3100	2980
M2–F–A10–CF	Full	10%	800 (Full height)	3080	2980
M3–F–A5–CN	Full	5%	–	3080	3000
M4–F–A5–CF	Full	5%	800 (Full height)	3100	3020
M5–H–A10–CH	Half	10%	400 (Half height)	3080	3060
M6–H–A10–CF	Half	10%	800 (Full height)	3080	3060
M7–H–A10–C100	Half	10%	100	3080	3060
M8–H–A5–C100	Half	5%	100	3080	3060
M9–H–A5–CH	Half	5%	400 (Half height)	3100	3060
M10–H–A5–CF	Half	5%	800 (Full height)	3100	3080

M1–F–A10–CN: Model 1 (model number); F: Fully filled; A10: 10% acid solution (5 for 5% and 10 for 10%); CN: No–CFRP coating (N for none, H for half of cylinder height, F for full height of cylinder and 100 for 100 mm as height of CFRP, at the middle height of cylinder)

Table 2. Properties of epoxies.

Material	Density (kg/l)	Bending strength (N/mm^2)	Compression strength (N/mm^2)
Epoxy resin adhesive	1.02	> 50	> 60
Epoxy resin primer	1.08	> 20	–

were mixed at a ratio of 1:2.22. After waiting 24 hours for primer to dry, MasterBrace 4500 branded special epoxy adhesive was applied to the cylinders' surface. Properties of the epoxies used in this research are given in Table 2. Then, appropriate sizes of CFRP were cut and placed on the surface of the model cylinders. The CFRP was wrapped on the surface and epoxy adhesive was applied again. Like the epoxy primer, it takes 24 hours for epoxy adhesive to get dry. In this study, cylinders were only coated with one layer of CFRP. CFRP fabrics used in this study are made of unidirectional and continuous fibers. Other properties of the CFRP fabrics used in this research are presented in Table 3.

Table 3. Properties of CFRP fabrics used in experiments.

Property	Value
Modulus of elasticity	230,000 N/mm^2
Ultimate tensile strength	4900 N/mm^2
Thickness	0.111 mm
Weight	230 g/m^2
Ultimate strain	2.1%
Width	500 mm

2.4. The buckling tests

At the last stage, models were placed in the test setup and the contact areas of the rollers with the set setup were glued with silicon to prevent air leaks. External pressure was applied to the cylinders with a vacuum pump that had a hydrostatic pressure capacity of 600 kPa, shown in Figure 3. Four SDP-300 branded Linear Variable Displacement Transducers (LVDT) used to measure the displacements on the cylinders occurring at different points with external pressure. The LVDTs used in this research can measure the displacements up to 300 mm. LVDTs are labeled as LVDT 1, LVDT 2, LVDT 3, LVDT 4 and the location of LVDTs is shown in Figure 3. Furthermore, the heights of LVDTs are presented in Table 4.

Two TML YEFLA-5 (5 mm $\times$ 3 mm dimensions, resistance value of 121 $\Omega \pm 0.5\%$, and sensitivity coefficient $2.1 \pm 2\%$) model strain gauges were used to determine the strain changes in the system. Strain gauges are labeled as VS and HS (VS: Vertical Strain and HS: Horizontal Strain). Heights of strain gauges are presented in Table 4. Since strain gauges measured the strains in the elastic region, they played an important role in determining the initial buckling of the cylinders. The cylinder surface was carefully cleaned before gluing the strain gauges. Then, the strain gauges were

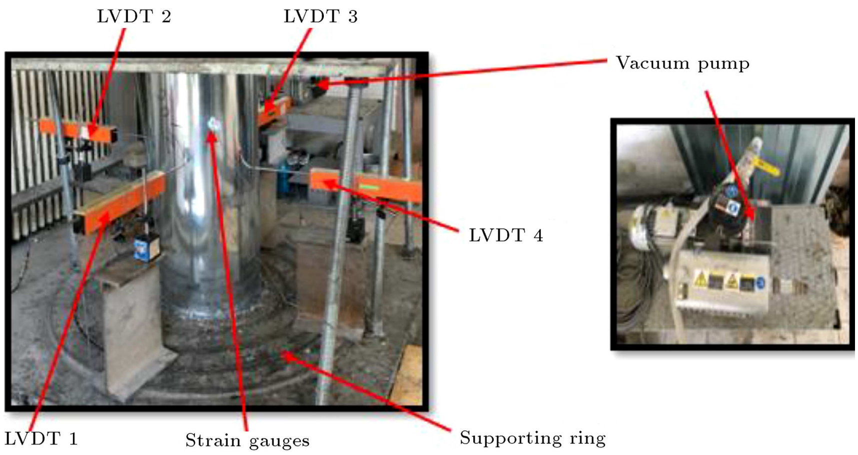

Figure 3. Overall view of the system.

Table 4. The properties of the measurement system.

Models	**Position of the device from ground (mm)**	
	For the LVDTs	**For the strain gauges**
Perfect model	480	600
Perfect model with whole surface CFRP	460	580
M1–F–A10–CN	500	620
M2–F–A10–CF	500	570
M3–F–A5–CN	470	580
M4–F–A5–CF	480	590
M5–H–A10–CH	470	610
M6–H–A10–CF	460	550
M7–H–A10–C100	480	550
M8–H–A5–C100	460	570
M9–H–A5–CH	500	580
M10–H–A5–CF	470	540

glued vertically and horizontally with fast adhesive. During the experiment, the behavior of the models was recorded with a camera. The exact time when the initial, overall, and collapse buckling took place and the locations of the buckling were determined by strain gauges, LVDTs, and camera recordings. The mentioned experimental settings were designed according to considerations of Teng et al. [37].

3. Test results

3.1. Theories for obtaining the buckling load and approximate waves

Buckling loads of the cylinders were calculated by Jawad, Venstel and Krauthammer, Ross theories and compared with the values obtained as a result of the experiment. According to Jawad's theory [32]:

$$P_{cr} = \frac{0.92E\left(\frac{t_e}{R}\right)^{2.5}}{\frac{L_e}{R}}. \tag{1}$$

According to Venstel and Krauthaer' theory [33]:

$$P_{cr} = 0.92\frac{Et}{L}\left(\frac{t}{r_m}\right)^{1.5}. \tag{2}$$

According to Ross' theory [34]:

$$P_{cr} = \frac{2.6E\left(\frac{t}{d}\right)^{2.5}}{\frac{H}{d} - 0.45\left(\frac{t}{d}\right)^{0.5}}, \tag{3}$$

where:

P_{cr}	The critical buckling load for the cylinders,
E	Modulus of elasticity (Young's modulus) = 210 GPa,
$t = t_e$	The effective thickness = 0.45 mm,
d	The diameter of the cylinder = 400 mm,
$R = r_m$	The radius of the cylinder = 200 mm,
$H = L_e = L$	The length of the cylinder = 800 mm.

Table 5. Buckling loads, experimental waves, and approximate waves.

	Specimens	Initial buckling (kPa)	Overall buckling (kPa)	Collapse buckling (kPa)	Experimental waves	Approximate waves [20,37]
Not Corroded specimens	Perfect model	40.85	95.63	93.05	5	6–7
	Perfect model with CFRP	120.19	165.68	115.46	4	6–7
Corroded specimens	M1–F–A10–CN	32.00	96.07	70.63	5	6–7
	M2–F–A10–CF	43.35	207.11	108.09	4	6–7
	M3–F–A5–CN	34.43	81.47	63.93	4	6–7
	M4–F–A5–CF	57.58	195.98	106.54	3	6–7
	M5–H–A10–CH	47.77	141.86	84.05	4	6–7
	M6–H–A10–CF	70.85	236.53	166.71	3	6–7
	M7–H–A10–C100	43.42	104.40	87.37	4	6–7
	M8–H–A5–C100	50.06	112.23	94.01	4	6–7
	M9–H–A5–CH	71.52	159.56	131.24	4	6–7
	M10–H–A5–CF	86.41	198.56	137.95	4	6–7

Figure 4. Models before and after buckling tests.

Buckling load was found 11.6 – 11.6 – 11.72 kPa according to Eqs. (1)-(4) relatively. Approximate number of circumferential buckling waves with external pressure was calculated by Fatemi et al. [20], Teng et al. [37]:

$$n = 2.74\sqrt{\frac{R}{L}\sqrt{\frac{R}{t}}}. \tag{4}$$

In Eq. (4), n expresses the approximate buckling waves, R the radius of the cylinder, t the thickness, and L the height of the cylinder. From Eq. (4), the approximate number of buckling waves was calculated as $6.29 \approx 6-7$, as shown in Table 5.

3.2. Buckling load of the models

The photos of the models before and after the tests are given in Figure 4. Pressure-displacement and buckling load-strain curves of all the models are shown in Figures 5 and 6. Each of the breaks in the buckling load-displacement curves represents one or more waves. Initial buckling is the first buckling wave that occurs at the end of the elastic zone. The first break of the curves in Figure 5 shows the initial buckling of cylinders. After initial buckling, cylinders resisted and carried more load without any air leaks. The buckling capacity of cylinders increased continuously until overall buckling. Overall buckling load expresses the ultimate carrying capacity of cylinders, and it is the highest value on the buckling load-displacement curves in Figure 5. Between the initial and overall buckling processes, more buckling waves occurred. First break of the curves in load-displacement figures after overall buckling represents the collapse buckling of cylinders. A figure that shows the location of these buckling phases on a graphic is

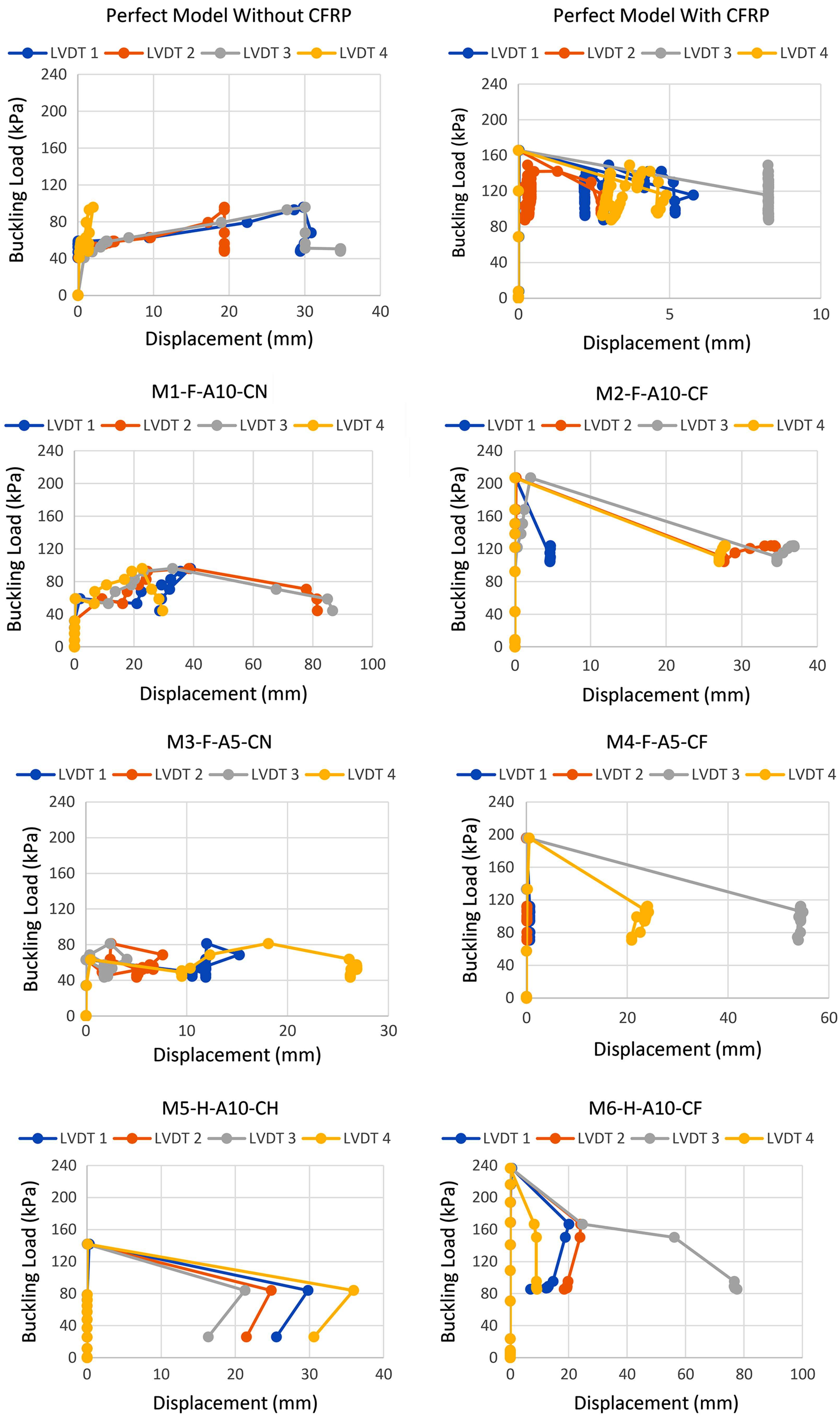

Figure 5. Buckling load-displacement curves of all specimens.

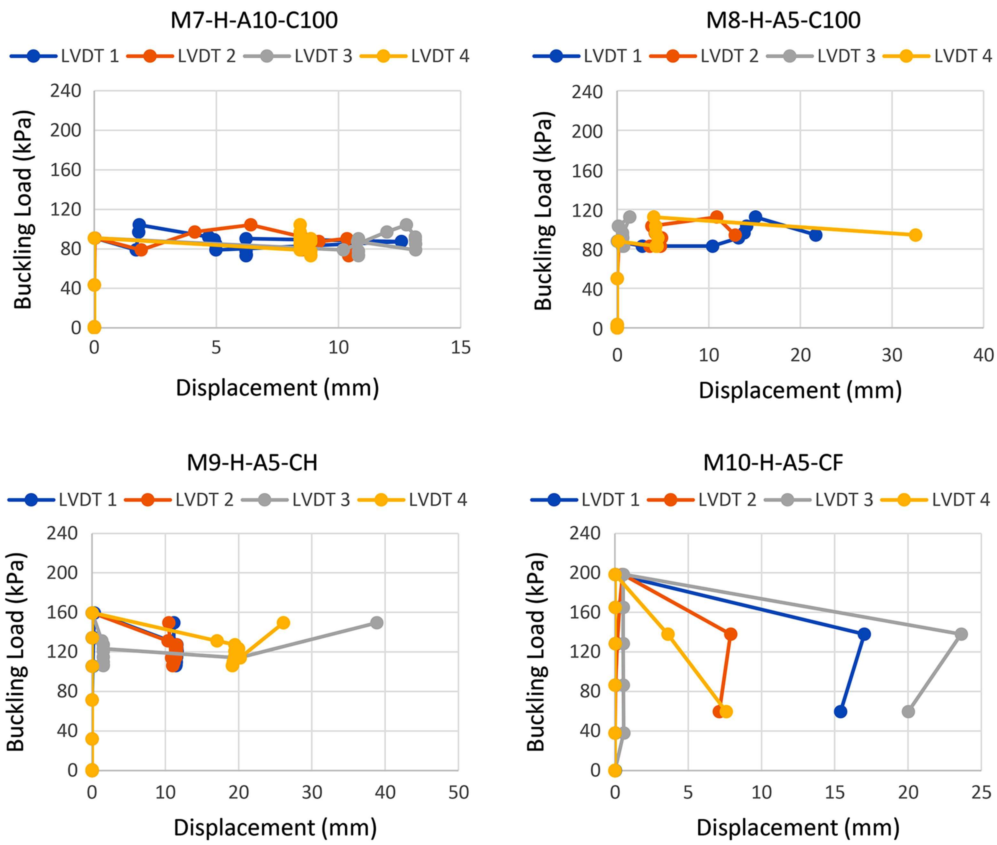

Figure 5. Buckling load-displacement curves of all specimens (continued).

given in Figure 7. The initial buckling, overall buckling, and collapse buckling values of the cylinders are given in Table 5 and shown in Figure 8. In Figure 8, arrows near the columns show the increase and decrease in the bucking loads. Under external pressure, it has been observed that HSs are larger than VSs. This can be explained by the size and corrosion effect. Strains were elastic until collapse and at a point of collapse, it was observed that the strains changed from elastic into plastic. The cylinders did not exhibit any buckling behavior before the first buckling and after the first buckling, they moved to the post-buckling stage. The rate of increase in buckling capacity varies between 1.38 and 4.78 times of the initial buckling. The overall buckling loads range from 27.46% to 79.07% compared to the initial buckling. The collapse buckling loads ranged between −4.09% and 57.5% compared to initial buckling.

The initial buckling load of the perfect model is presented in Table 5 and Figure 5. Table 6 shows the change of buckling loads compared to the initial buckling for each model. The overall buckling capacity of the perfect model is 2.34 times greater than the initial buckling, and the collapse buckling is 2.28 times greater than the initial buckling load. The overall buckling is increased by 57.28% and the collapse buckling load is increased by 56.1% compared to the first buckling. In the perfect model with the whole surface CFRP, the overall buckling load is 1.38 times greater than the initial buckling and the collapse buckling is 0.96 times greater than the initial buckling. The overall buckling capacity increases by 27.46% and the collapse buckling capacity decreases by 4.1% compared to the initial buckling. For this group, the perfect model without CFRP has the greatest increase at the post-buckling phase. The initial buckling capacity of the perfect model without CFRP is reduced by 66% compared to perfect model with CFRP. When these two models are compared, it is seen that the initial buckling capacity of the cylinder with CFRP is 2.94 times greater than the initial buckling capacity of the cylinder without CFRP. According to these data, the application of CFRP to the cylinders can increase the initial buckling capacity up to 300%.

For the M1-F-A10-CN model fully filled with 10% acid solution, the overall buckling was found to be 3 times greater than the initial buckling and the collapse buckling was 2.21 times greater than the initial buckling. The overall buckling increased by 66.69% while the collapse buckling increased by 54.69% compared to the initial buckling. The initial buckling capacity of M1-F-A10-CN is reduced by 21.66% compared to the perfect one without CFRP. The corrosion reduced the initial buckling capacity of the model. For the model

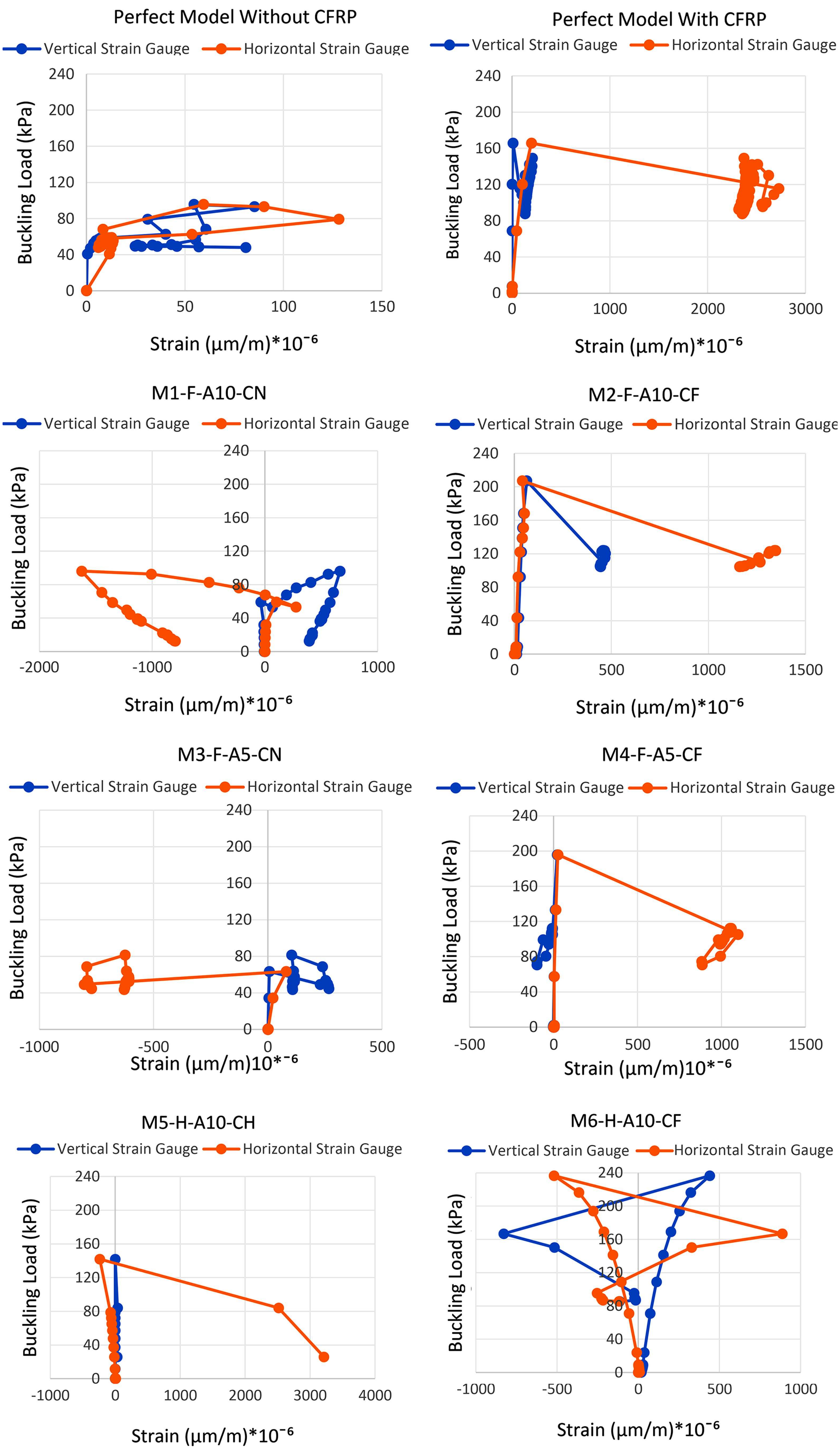

Figure 6. Buckling load-strain curves of all specimens.

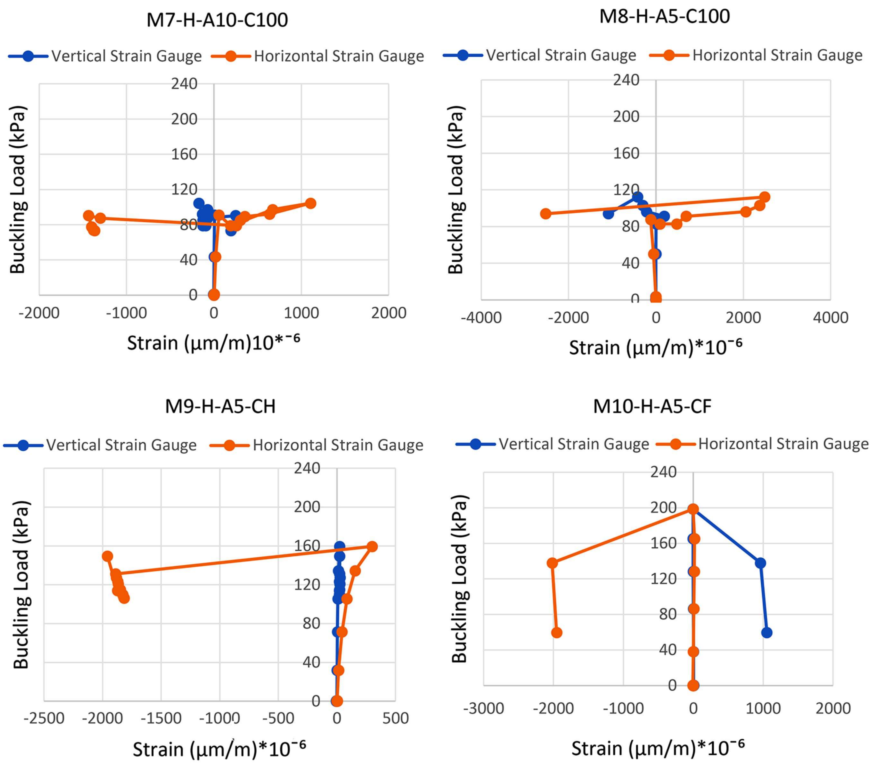

Figure 6. Buckling load-strain curves of all specimens (continued).

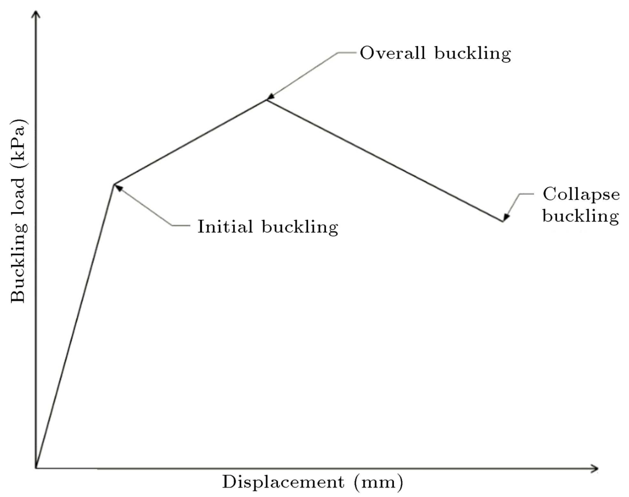

Figure 7. Locations of the buckling phases.

M2-F-A10-CF, which was filled with the same amount of acid solution, but tested with CFRP reinforcement on the entire surface, overall buckling was found 4.78 times the initial buckling and collapse buckling was found 2.49 times the initial buckling. For this model, the overall buckling increased by 79.07% and the collapse buckling increased by 59.89% compared to the initial buckling. For this group, the model M2-F-A10-CF caused the greatest increase at the post-buckling phase. Initial buckling capacity of M2-F-A10-CF decreased by 63.93% compared to the perfect model with CFRP. Upon the comparison of these two models, it was seen that the initial buckling capacity of the model with CFRP was 1.35 times more than the model without CFRP.

For the M3-F-A5-CN fully filled with the acid ratio 5%, the overall buckling was found 2.37 times the initial buckling and the collapse buckling was 1.86 times the initial buckling. The overall buckling increased by 57.74% and the collapse buckling increased by 46.14% compared to the initial buckling. Initial buckling capacity of the M3-F-A5-CN model decreased by 15.72% compared to the model without CFRP. For the M4-F-A5-CF model filled with the same amount of acid solution, but tested with CFRP reinforcement on the entire surface, overall buckling was found to be 3.4 times initial buckling and collapse buckling was found to be 1.85 times the initial buckling. The overall buckling increased by 70.62% and the collapse buckling increased by 45.95% compared to the initial buckling for this model. The initial buckling capacity of the M4-F-A5-CF model decreased by 52.08% compared to the perfect one with CFRP. For this group of models, the model M4-F-A5-CF had the greatest increase at the post buckling phase. When these two models were compared, it was seen that the initial buckling capacity of the model with CFRP was 1.67 times more than the one without CFRP.

In the M5-H-A10-CH model, which was half-filled with 10% acid solution and coated with CFRP along the corroded part (up to half the cylinder height), the overall buckling was found to be 2.97 times the

Table 6. Increase and decrease of the buckling loads of the models compared to initial buckling.

	Specimens	$\frac{\text{Overall}-\text{Initial}}{\text{Overall}}$ (%)	$\frac{\text{Collapse}-\text{Initial}}{\text{Collapse}}$ (%)
Not Corroded specimens	Perfect model	57,28	56,1
	Perfect model with CFRP	27,46	–4,1
Corroded specimens	M1–F–A10–CN	66,69	54,69
	M2–F–A10–CF	79,07	59,89
	M3–F–A5–CN	57,74	46,14
	M4–F–A5–CF	70,62	45,95
	M5–H–A10–CH	66,33	43,16
	M6–H–A10–CF	70,05	57,5
	M7–H–A10–C100	58,41	50,3
	M8–H–A5–C100	55,4	46,75
	M9–H–A5–CH	55,18	45,5
	M10–H–A5–CF	56,48	37,36

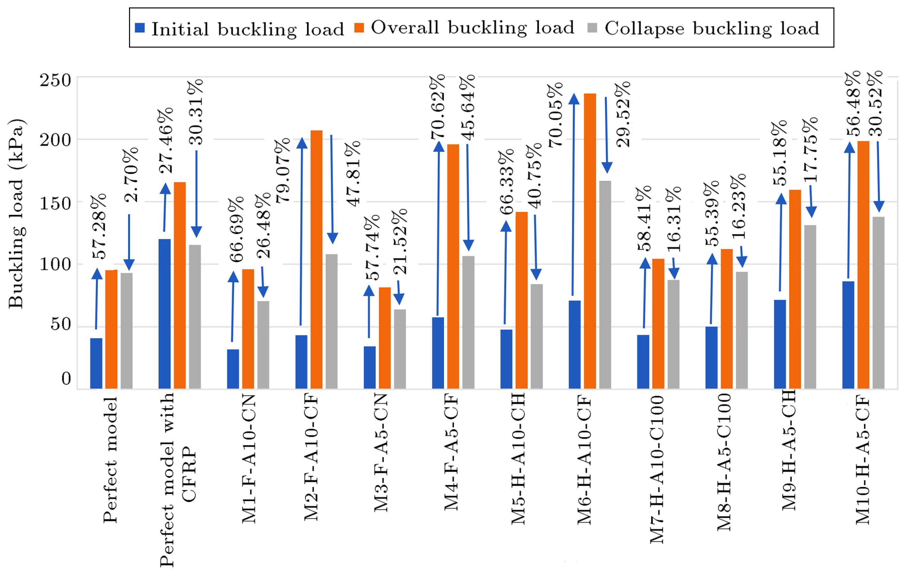

Figure 8. Initial, overall, and collapse buckling loads of the models.

initial buckling and collapse buckling was found to be 1.76 times the initial buckling. The overall buckling increased by 66.33%, and the collapse buckling increased by 43.16% compared to the initial buckling. Initial buckling capacity of the M5-H-A10-CH increased by 14.48% and decreased by 60.25%, when compared to perfect model without and with CFRP, respectively. For the model M6-H-A10-CF, which was half-filled with the same amount of acid solution, but tested with CFRP strengthening on the entire surface of the cylinder, the overall buckling was found to be 3.34 times the initial buckling and collapse buckling was found to be 2.35 times the initial buckling. The overall buckling increased by 70.05%, and the collapse buckling increased by 57.5% compared to the initial buckling for this model. The initial buckling capacity of the M6-H-A10-CF increased by 42.34% and decreased by 41.04% compared to the perfect model without and with CFRP, respectively. For the model M7-H-A10-C100, the overall buckling was found 2.4 times the initial buckling and the collapse buckling was found to be 2.01 times the initial buckling. The overall buckling increased by 58.41% and the collapse buckling increased by 50.3% compared to initial buckling. With 100 mm CFRP coating, the initial buckling capacity increased by 5.92% and decreased by 63.87% compared to the perfect model without CFRP and perfect model with CFRP, respectively. Based on the comparison of these three models, it was observed that the initial buckling capacity of the model with full CFRP was 1.48 times greater than the model with half-surface CFRP and 1.63 times more than the model with 100 mm CFRP. Initial buckling capacity of the M5-H-A10-CH decreased by 32.57% compared to the M6-H-A10-CF. The initial buckling capacity of the M7-H-A10-C100 was decreased by 38.71% and 9.1% compared to the M6-H-A10-CF and the M5-H-A10-CH, respectively. For this group, the model M6-H-A10-CF and the M7-H-A10-C100 had the most and least rates of increase at the postbuckling phase.

For the model M8-H-A5-C100, which was tested by half filling with 5% acid solution and strengthened with 100 mm CFRP, overall buckling was found 2.24 times the initial buckling and collapse buckling was found 1.88 times the initial buckling. For this model, overall buckling increased by 55.4% of the initial buckling and the collapse buckling increased by 46.75% of the initial buckling. The initial buckling capacity of the M8-H-A5-C100 increased by 18.4% and decreased by 58.35% compared to the perfect model without CFRP and perfect one with CFRP, respectively. For the M9-H-A5-CH in which CFRP reinforcement was applied only to corroded zones (half length of the cylinder), the overall buckling was found 2.23 times the initial buckling and the collapse buckling was found 1.84 times the initial buckling. The overall buckling increased by 55.18% and the collapse buckling increased by 45.5% when compared to initial buckling. The initial buckling capacity of the model M9-H-A5-CH increased by 42.88% and decreased by 40.49% compared to the perfect model without CFRP and the perfect one with CFRP, respectively. For the M10-H-A5-CF model, which was half-filled with 5% acid solution and tested with the whole-surface CFRP, overall buckling was found 2.3 times the initial buckling and collapse buckling was found 1.6 times the initial buckling. The overall buckling increased by 56.48% and the collapse buckling is increased by 37.36% compared to initial buckling, respectively. The initial buckling capacity of the M10-H-A5-CF increased by 52.72% and decreased by 28.1% compared to the perfect one without CFRP and the perfect model with CFRP, respectively. Based on the comparison of these three models, it was observed that the initial buckling capacity of the model with full CFRP was 1.21 times greater than the model with half CFRP and 1.73 times more than the model with 100 mm CFRP. The initial buckling of M10-H-A5-CF increased by 42.06% and 17.23% compared to the model M8-H-A5-C100 and the model M9-H-A5-CH, respectively. The initial buckling capacity of the M9-H-A5-CH increased by 30% compared to the model M8-H-A5-C100. For this group, the M10-H-A5-CF and M9-H-A5-CH models had the greatest and least rates of increase at the postbuckling phase.

3.3. Comparison of the models with same height of CFRP

The initial buckling of the models without CFRP presented a 7% decrease for the increased acid solution ratio from 5 to 10% for the M3-F-A5-CN and M1-F-A10-CN models. However, this decrease is about 25% for the wholly CFRP-covered M4-F-A5-CF and the M2-F-A10-CF models.

As expected, the decrease for the models covered with only 100 mm is about 13% for the M7-H-A10-C100 and the M8-H-A5-C100. Furthermore, the half-length models coated with CFRP presented a similar behavior for the M9-H-A5-CH and M5-H-A10-CH models; to be specific, following a 33% decrease in the initial buckling, the acid solution increased. Nevertheless, this decrease was about 18% for the fully coated, but half-acid-solution-filled models, i.e., M10-H-A5-CF and M6-H-A10-CF. According to these results, increasing the ratio of acid to 10% increased the damage caused by corrosion. As the acid ratio increases, initial buckling capacity of thin-walled cylindrical shells decreases, as expected.

3.4. Comparison of the models with the same acid ratio

Among the models containing 10% acid, M2-F-A10-CF and M7-H-A10-C100 had the greatest and least rates of increase in the post-buckling capacity after the initial buckling. The initial buckling capacity of the model M2-F-A10-CF decreased by 38.31%, when compared to the M6-H-A10-CF. Among the models containing 5% acid, M4-F-A5-CF and M9-H-A5-CH had the greatest and least rates of increase in the post-buckling capacity after initial buckling. The initial buckling capacity of the model M4-F-A5-CF decreased by 33.36%, when compared to the model M10-H-A5-CF. These results show that as the fullness of the cylinders' increases, the buckling capacity decreases. The models filled with more HCl solutions have lower buckling capacities, as expected.

3.5. Failure modes

Table 5 shows the number of experimental waves and approximate waves according to [20,37]. The waves ranged between 3 and 5. The theoretically calculated number of waves was greater than that of experimental waves. The models after the test are shown in Figure 4. The buckling failure of all models occurred at the bottom and top of the cylinders. For the uniform external pressure, V-shaped buckle lines occurred. The models with CFRP were more resistant to buckling. The CFRP coating increased the buckling resistance of the cylinders strikingly.

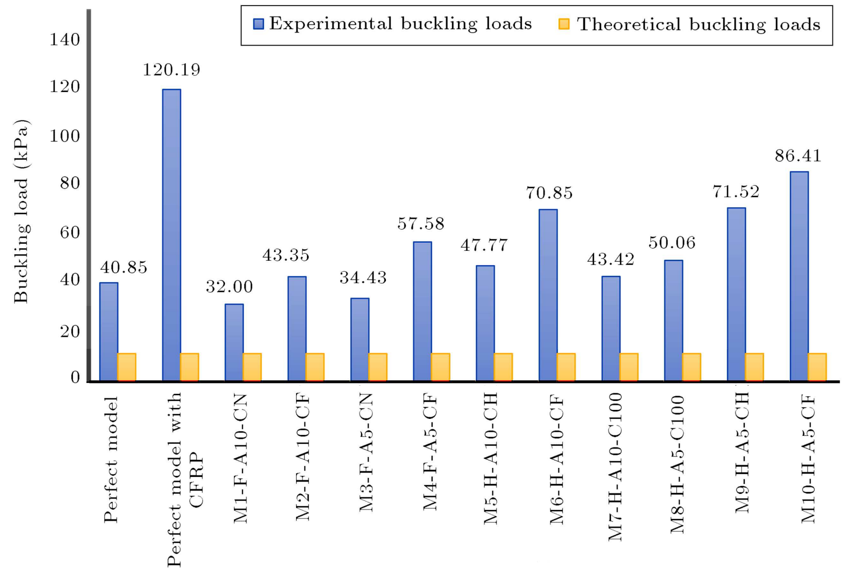

Figure 9. Comparison of initial and theoretical buckling loads.

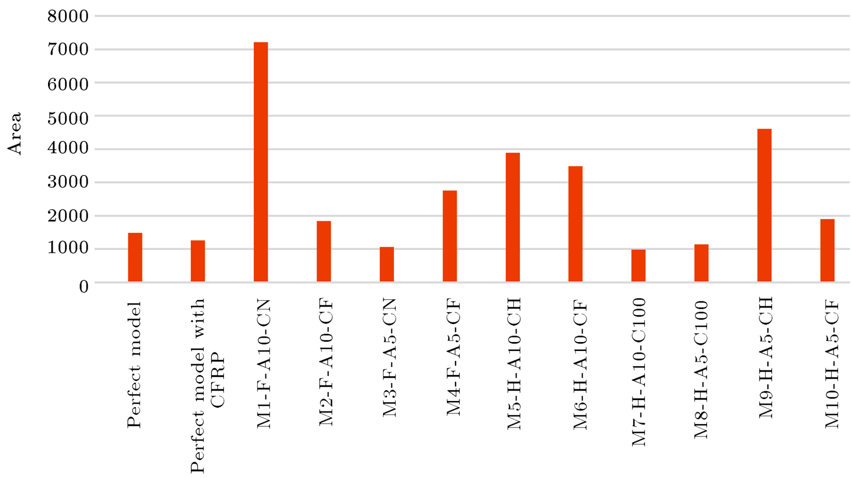

Figure 10. Areas under pressure-displacement curves for all models.

3.6. Comparing the theoretical and experimental buckling loads

Buckling loads were found as 11.6, 11.6, and 11.72 kPa according to similar theories like Jawad's theory, Venstel and Krauther's theory, and Ross' theory, respectively. The experimental buckling loads are presented in Table 5. The comparisons of experimental initial buckling loads of every model with theoretical loads are shown in Figure 9. Theoretical loads are smaller than the experimental ones. The buckling loads according to these theories do not include the effect of corrosion and they should be multiplied by certain coefficients.

3.7. Energy absorption capacity of models

Areas under the buckling load-strain curves are presented in Figure 10. This area represents the ductility of the cylinders as they can absorb more energy. The model M1-F-A10-CN had the largest area among all the models. By coating the cylinders with CFRP, buckling load increases significantly and it also increases the ductile behavior of cylinders. Ductility is an important feature of shell design because it allows shells to carry more loads by increasing their deformability. Deformability is also related to ductility. As the energy absorption capacity of shells increases, deformability and load-carrying capacity also increase. With more ductility, shells can keep carrying loads by changing their shape more.

4. Conclusion

The corrosion can be a big problem for the thin-walled storage members. In particular, the storage of liquids, which decreases the pH value by time, resulted in corroded thin-walled steel shells. Thus, as a purpose of this work, the corrosion of the models was intensively investigated. The corroded thin-walled cylindrical steel shells were experimentally tested by using 12 thin-walled cylindrical shells, corroded ten and non-corroded two models, and subjected to external pressure. The key findings and observations of this study are presented as follows:

- All models experienced resistance after initial buckling and then, they exhibited the post-buckling behavior. The comparisons of overall and collapse buckling with initial buckling were observed in the range of 67%–79% and 55%–60%, respectively, for fully filled models with 10% HCl. Relevant observations for 5% HCL were observed in the range of 58%–71%, and 46%, respectively;
- The comparison of half-filled models evaluated the overall and collapse buckling with initial buckling between 58%–70% and 43%–58%, respectively, for the 10% HCL ones. Relevant observations for 5% HCL are observed within the range of 55%–57%. The Carbon Fiber-Reinforced Polymer (CFRP) coating significantly increased the initial buckling capacity of the models;
- The models lost weight due to corrosion thickness loss effect. For the models fully filled with 10% HCl solutions and those half-filled, the weight loss was about 4% and 1%, respectively. Furthermore, fully filled 5% HCl solution models lost about 3% of their weight and half-filled ones lost about 1% of their weight. Thickness loss caused the buckling load to decrease in all models;
- Filling the cylinders with more solution caused buckling capacity to decrease. The models filled with more HCl solution had lower buckling capacities;
- The acid ratio of the solution affected the damage caused by corrosion. As the acid ratio increased, initial buckling capacity of thin-walled cylindrical shells decreased;
- Upon the comparison of the experimental results, it was found that the theoretical results could be used to evaluate the loads of the models based on certain coefficients; however, the theories were not determined for the purpose;
- By coating the cylinders with CFRP, buckling load increased significantly and it also increased the ductility of cylinders.

Acknowledgment

The research is part of the Ataturk University Projects No: FHD-2019-7272 and FHD-2019-7344. The authors would like to thank Ataturk University for funding the project.

References

1. Schweitzer, P.A., *Fundamentals of Corrosion*, CRC Press, USA (2010).
2. Sharifi, Y. and Rahgozar, R. "Remaining moment capacity of corroded steel beams", *International Journal of Steel Structures*, **10**, pp. 165–176 (2010).
3. Wang, Y., Xu, S., Wang, H., et al. "Predicting the residual strength and deformability of corroded steel plate", *Construction and Building Materials*, **152**, pp. 777–793 (2017).
4. Cinitha, A., Umesha, P.K., and Iyer, N.R. "An overview of corrosion and experimental studies on corroded mild steel compression members based on the corrosion Morphology", *KSCE Journal of Civil Engineering*, **18**(6), pp. 1735–1744 (2014).
5. Sharifi, Y. and Rahgozar, R. "Evaluation of the remaining shear capacity in corroded steel I-beams", *Advanced Steel Construction*, **6**(2), pp. 803–816 (2010).
6. Lugauskas, A., Bikulčius, G., Bučinskien0̆117, D., et al. "Long-time corrosion of metals (steel and aluminium) and profiles of fungi on their surface in outdoor environments in Lithuania", *CHEMIJA*, **27**(3), pp. 135–142 (2016).
7. Çelik, Ö, *The Effect of Low Temperature Nitriding on Mechanical and Corrosion Properties of Stainless Steels*, Istanbul Technical University, Turkey (2010). (in Turkish)
8. Qiao, W. "Water pipeline failures: Field verification and risk-based corrosion-fracture models", *University of Houston*, USA (2011).
9. Manliza, C.W.M. "A critical study on corrosion and corrosion control methods for piping systems in Hong Kong", *The Hong Kong Polytechnic University*, China (2003).
10. Becerra, H.Q., Retamoso, C., and Macdonald, D.D. "The corrosion of carbon steel in oil-in-water emulsions under controlled hydrodynamic conditions", *Corrosion Science*, **42**, pp. 561–575 (2000).
11. Patané, G., Proverbio, E., and Risitano, A. "Corrosion induced failure of an air cylinder", *Engineering Failure Analysis*, **9**, pp. 481–487 (2002).
12. Kong, X., Lv, J., Gao, N., et al. "An experimental study of galvanic corrosion on an underwater weld joint", *Journal of Coastal Research*, **84**, pp. 63–68 (2018).
13. Chegeni, B., Jayasuriya, S., and Das, S. "Effect of corrosion on thin-walled pipes under combined internal pressure and bending", *Thin-Walled Structures*, **143**, p. 106218 (2019).
14. Zhao, Z., Liang, B., Liu, H., et al. "Influence of pitting corrosion on the bending capacity of thin-walled circular tubes", *Journal of the Brazilian Society of Mechanical Sciences and Engineering*, **40**(548), pp. 1055–1064 (2018).

15. Taraghi, P., Showkati, H., and Firouzsalari, S.E. "The performance of steel conical shells reinforced with CFRP laminates subjected to uniform external pressure", *Construction and Building Materials*, **214**, pp. 484–496 (2019).

16. Kabir, M.Z. and Nazari, A. "Experimental and numerical study on the nonlinear response of notched cylinders under compressive loading", *Scientia Iranica*, **19**(3), pp. 355–365 (2012).

17. Golzan, B.S. and Showkati, H. "Buckling of thin-walled conical shells under uniform external pressure", *Thin-Walled Structures*, **46**, pp. 516–529 (2008).

18. Maali, M., Aydın, A.C., Showkati, H., et al. "The effect of longitudinal imperfections on thin-walled conical shells", *Journal of Building Engineering*, **20**, pp. 424–441 (2018).

19. Kılıç, M., and Çinar, M. "Buckling behavior of sulfate-corroded thin-walled cylindrical steel shells reinforced with CFRP", *Iran J Sci Technol Trans Civ Eng.*, **45**, pp. 2267–2282 (2020).

20. Fatemi, S.M., Showkati, H., and Maali, M. "Experiments on imperfect cylindrical shells under uniform external pressure", *Thin-Walled Structures*, **65**, pp. 14–25 (2013).

21. Niloufari, A., Showkati, H., Maali, M., et al. "Experimental investigation on the effect of geometric imperfections on the buckling and post-buckling behavior of steel tanks under hydrostatic pressure", *Thin Walled Structures*, **74**, pp. 59–69 (2014).

22. Ghalghachi, R.N., Showkati, H., and Firouzsalari, S.E. "Buckling behavior of GFRP cylindrical shells subjected to axial compression load", *Composite Structures*, **260**, p. 113269 (2021).

23. Maghsoudi, A.A. and Bengar, H.A. "Acceptable lower bound of the ductility index and serviceability state of RC continuous beams strengthened with CFRP sheets", *Scientia Iranica*, **18**(1), pp. 36–44 (2011).

24. Zojaji, A.R. and Kabir, M.Z. "Analytical approach for predicting full torsional behavior of reinforced concrete beams strengthened with FRP materials", *Scientia Iranica*, **19**(1), pp. 51–63 (2012).

25. Mortezaei, A. and Ronagh, H.R. "Plastic hinge length of FRP strengthened reinforced concrete columns subjected to both far-fault and near-fault ground motions", *Scientia Iranica*, **19**(6), pp. 1365–1378 (2012).

26. Teng, J.G., Yu, T., and Fernando, D. "Strengthening of steel structures with fiber-reinforced polymer composites", *Journal of Constructional Steel Research*, **78**, pp. 131–143 (2012).

27. Deng, J., Li, J., Wang, Y., et al. "Numerical study on notched steel beams strengthened by CFRP plates", *Construction and Building Materials*, **163**, pp. 622–633 (2018).

28. Li, A., Xu, S., Wang, H., et al. "Bond behavior between CFRP plates and corroded steel plates", *Composite Structures*, **220**, pp. 221–235 (2019).

29. Maali, M., Kılıç, M., Yaman, Z., et al. "Buckling and post-buckling behavior of various dented cylindrical shells using CFRP strips subjected to uniform external pressure: Comparison of theoretical and experimental data", *Thin-Walled Structures*, **137**, pp. 29–39 (2019).

30. Teng, J.G. and Hu, Y.M. "Behavior of FRP-jacketed circular steel tubes and cylindrical shells under axial compression", *Construction and Building Materials*, **21**, pp. 827–838 (2007).

31. Ghazijahani, T.G., Jiao, H., and Holloway, D. "Timber filled CFRP jacketed circular steel tubes under axial compression", *Construction and Building Materials*, **94**, pp. 791–799 (2015).

32. Jawad, M.H. "Theory and design of plate and shell structures", Chapman and Hall, UK (1994).

33. Venstel, E. and Krauthammer, T. "Thin plates and shells: Theory: Analysis, and applications", *Marcel Dekker Inc.*, New York, USA (2001).

34. Ross, C.T.F. "A proposed design chart to predict the inelastic buckling pressures for conical shells under uniform external pressure", *Mar. Technol.*, **44**(2), pp. 77–81 (2007).

35. Maali, M., Aydın, A.C., and Sağıroğlu, M. "Investigation of innovative steel runway beam in industrial building", *Sādhanā*, **40**(7), pp. 2239–2251 (2015).

36. Aydın, A.C., Maali, M., Kılıç, M., et al. "Experimental investigation of sinus beams with end-plate connections", *Thin-Walled Structures*, **97**, pp. 35–43 (2015).

37. Teng, J.G., Zhao, Y., and Lam, L. "Techniques for buckling experiments on steel silo transition junctions", *Thin-Walled Structures*, **39**, pp. 685–707 (2001).

Biographies

Abdulkadir Cüneyt Aydin is a Professor at the Department of Civil Engineering, Atatürk University, Turkey. He is a Member of Engineering Faculty Research Commission and also, the Head of the Department of Civil Engineering Structural Engineering Division. His research focuses are steel constructions, thin-walled structures, structure strengthening, construction materials, and reinforced concrete structures. He is a well-known researcher with his published articles and conference papers. He is also the chief editor and an editorial board member of many international scientific journals.

Mahmut Buğra Bilen is a Research Assistant at the Department of Civil Engineering, Erzurum Technical University, Turkey. He studied Civil Engineering at Ataturk University, Turkey and he is currently studying for his MSc degree at the same university. His research interests include thin-walled steel structures.

Mahyar Maali is an Associate Professor at the Department of Civil Engineering, Erzurum Technical University, Turkey. He studied Civil Engineering at Islamic Azad University, Maragheh, Iran and he obtained his MSc from the same university. Then, he studied for his PhD at the Department of Civil Engineering, Ataturk University, Turkey. His research interests are mostly about steel structures.